Article:
Girimonte, R, Vivacqua, V and Formisani, B (2016) Extension of the model of binary fluidization to beds confined in a packing of coarse spheres. Powder Technology, 297. pp. 275-282. ISSN 0032-5910

https://doi.org/10.1016/j.powtec.2016.04.034

EXTENSION OF THE MODEL OF BINARY FLUIDIZATION TO BEDS CONFINED IN A PACKING OF COARSE SPHERES

Rossella Girimonte[1]*, Vincenzino Vivacqua[2] , Brunello Formisani[1]

[1]Dipartimento di Ingegneria per l'Ambiente e il Territorio e Ingegneria Chimica,

Università della Calabria; I 87030 Arcavacata di Rende (Cosenza), Italy

[2]Center for Advanced Materials, Qatar University, Doha 2713, Qatar

*T: +39-0984-496689; F: +39-0984-496655; E: rossella.girimonte@unical.it

ABSTRACT

The prediction of the minimum fluidization velocity of beds of Geldart's group B particles confined in a packed bed of coarse spheres can be achieved by extending to this peculiar type of systems the theory developed for modelling the behaviour of segregating beds of simultaneously fluidized solids.

The approach is based on separate force balances on the fluid and the fine solids, capable to account for the peculiar nature of solid-solid interaction in a confined fluidized bed. Its validation is fulfilled by an extended investigation conducted in two columns (5 and 10 cm OD) packed with a fixed bed of 4.1 mm lead shots or 11 mm glass beads. The effect of particle size on the fluidization regime is investigated by comparing the results provided by experiments in which various cuts of glass ballotini, ranging from 100 to nearly 600 μm, are fluidized in two packings of fixed spheres; possible differences of behaviour due to particle density are analysed by series of experiments employing particles of ceramics, zirconium oxide, steel and bronze of the same diameter.

The results obtained confirm the effectiveness of the approach followed, in which an important role is played by the indirect interaction between the two solid phases.

KEYWORDS

Confined-fluidized beds; bubble-free fluidization; packed-fluidized beds; binary fluidization; solid interaction.

1. INTRODUCTION

Fluidization of multicomponent beds has been employed in a large number of processes. In most cases the different solid species are brought into the fluidized state simultaneously, such as in combustion or gasification processes. A distinctive feature of these systems is the often unavoidable tendency of the solid components to segregate, giving rise to a non-homogeneous internal composition of the bed [1-5]. It has recently been shown that a key-role is played by solid-solid interactions in the mechanisms of binary fluidization [6]. In that work, assessing the component contribution to the total pressure drop allowed writing separate force balances on each component of the multiphase system. By this way, the authors derived an expression for the interaction force and confirmed a criterion, available from the literature [7], capable of providing the initial segregation direction of each solid in a well-mixed bed upon incipient fluidization. The authors also argued that the presence of solid-solid interactions explains the gradual nature of binary fluidization, which is accomplished along a fluidization velocity interval [8, 9].

In other cases only one solid is to be fluidized, while the other component remains packed during the whole process. This system, often referred to as “packed-fluidized bed” or “confined fluidized bed” [10], has been raising an increasing interest as its fluid-solid contact mode is particularly suitable for operations in which maximization of the conversion of a gaseous reactant is crucial [11-13]. That is due to the ability of these fluidized systems to prevent the formation of bubbles, a route by which part of the gas feed by-passes the contact with the solid phase, whether it is another reactant or a catalyst.

A confined fluidized bed can be considered as a particular type of two-component mixture of solids, in which the interstitial network provided by the packed solid constitutes the confining environment in which the finer component achieves the suspended state and then expands without the formation of bubbles (Fig. 1). This fluidization technique seems likely to provide a very efficient

fluid-solid contact mode, suitable for high conversion of gaseous reactants, nearly complete adsorption of specific components of the fluidizing stream, filtration or heat recovery from dust-laden gases [14-22]. Contact efficiency of operations of this kind improves over a broad velocity range without the handling problems orderly associated to the use of fine powders. That is even more true for applications in which the solid of interest (for instance a sorbent or a catalyst) is a powder obtained from a synthesis, then granulated in nearly spherical pellets of larger size.

In a recent work [23], equations were derived and validated to predict the relationship between the degree of expansion of the fine solid and the operating fluidization velocity, namely the key-feature of the technique. However, the authors did not address the prediction of the minimum fluidization velocity of solids under confined conditions. Modelling the transition to the fluidized state of these systems will therefore be the objective of the present analysis, now made possible by the availability of a general theoretical model of the fluidization behaviour of two-solid systems. To this regard, the theory developed for segregating beds of simultaneously fluidized solids, that makes use of separate force balances for each of the phases of interest, will be extended to the homogeneous fluidization of Geldart's group B particles in a packed bed of coarse spheres.

2. THEORY

2.1 Separate force balances

Following what suggested by Wallis [24], separate force balances can be written for each component of the multiphase system. In the case of one-dimensional steady-state flow, for a binary solid bed the form of these equations is:

$$-\frac{dP}{dz} + b_i + f_i = 0 \qquad (1)$$

where b_i's are the body forces per unit volume on the i^{th} component and f_i's are the average surface forces per unit volume not contained in the pressure gradient. In a previous work [6], the term f_i in Eq. (1), written for the two solid species, comprised the pure drag force exerted by the fluid as well as the interaction forces between the two solids. For a bed of two simultaneously-fluidized solids, the force exerted by the packed component on the fluidized one (i.e. that with lower u_{mf}) delays its suspension. In other words, this force is responsible for the fact

that the initial fluidization velocity of a well-mixed two-solid bed is generally larger than u_{mf} of its "fluidized" component. However, the presence of this interaction requires that both solids can be suspended at the same time, i.e. that they have comparable minimum fluidization velocities; this happens when none of the two species forms an independent structure, i.e. a structure in which any pair of particles of either component is virtually connected by a path through the contact points between particles of the same kind.

In a packed-fluidized bed the coarse particles form an independent structure and their weight is therefore directly discharged on the distributor rather than being exerted on the other solid. As far as the particle size ratio d_p/d_f is not lower than about 10 [20], the interstitial voids of this structure provide the space in which the fine particles can move freely. Thus, in this case the interaction force in Eq. (1) is null. In light of these considerations, Eq. (1) can be particularized for the fluid phase and the two solid components; once that the finer particles are fluidized and homogeneously suspended such relationships are written as:

Fluid phase - gas (g)
$$-\frac{dP}{dz}-\rho_g g-180\frac{\mu_g u}{d_{av}^2}\frac{(1-\varepsilon)^2}{\varepsilon^3}=0 \tag{2}$$

Solid phase - fine component (f)
$$-\frac{dP}{dz}-\rho_f g+180\frac{\mu_g u}{d_{av}d_f}\frac{(1-\varepsilon)}{\varepsilon^2}=0 \tag{3}$$

Solid phase – packing (p)
$$-\frac{dP}{dz}-\rho_p g+180\frac{\mu_g u}{d_{av}d_p}\frac{(1-\varepsilon)}{\varepsilon^2}+f_d=0 \tag{4}$$

where d_{av} is the Sauter mean diameter [8, 9], defined as:
$$\frac{1}{d_{av}}=\frac{x_p}{d_p}+\frac{x_f}{d_f} \tag{5}$$

The fine solid fraction is
$$x_f=\frac{\alpha_f}{(\alpha_f+\alpha_p)}=\frac{\alpha_f}{(1-\varepsilon)} \tag{6}$$

with α_i calculated as
$$\alpha_p=\frac{m_p}{(\rho_p\ AH_p)}=(1-\varepsilon_p) \tag{7}$$

$$\alpha_f=\frac{m_f}{(\rho_f\ AH_{fc})} \tag{8}$$

so that

$$\varepsilon = (1-\alpha_p-\alpha_f) \tag{9}$$

In Eq (4) f_d is the unbalanced weight of the coarse particles (the packing) which is discharged on the distributor. In the force balances for the two solids, the drag force on each of them has been obtained from the Carman-Kozeny equation and partitioned according to their respective surface fractions [6].

2.2 Minimum fluidization velocity in confined conditions

As a result of having disregarded the interaction term between the two solids, the system of Eqs (2) and (3) can be solved separately. However, indirectly the two solids do interact in that each of them modifies the fluid flow field in which the other one is immersed. Solution of Eqs (2) and (3) gives the expressions of the gas velocity and pressure gradient:

$$u = u_{mfc} = \frac{(\rho_f - \rho_g) g d_{av}^2 \varepsilon^3}{180 \mu_g (1-\varepsilon)\left[(1-\varepsilon) + \varepsilon \frac{d_{av}}{d_f}\right]} \tag{10}$$

$$-\frac{dP}{dz} = \rho_g g + \frac{(\rho_f - \rho_g)(1-\varepsilon) g}{(1-\varepsilon) + \varepsilon \frac{d_{av}}{d_f}} \tag{11}$$

where u can be regarded as the minimum fluidization velocity in confined conditions, i.e. $u=u_{mfc}$. Substitution of Eqs (10) and (11) into Eq. (4) provides f_d which is, however, of limited interest. At large Reynolds numbers, employing the Ergun's relationship [25] for the frictional pressure drop leads to the following equation for the fluidization velocity:

$$\left[150 \frac{\mu_g (1-\varepsilon)}{\varepsilon^3 d_{av}^2} u_{mfc} + 1.75 \frac{\rho_g}{\varepsilon^3 d_{av}} u_{mfc}^2\right]\left[(1-\varepsilon) + \varepsilon \frac{d_{av}}{d_f}\right] = (\rho_f - \rho_g) g \tag{12}$$

Eqs (10) and (12) reduce to the conventional equation for the minimum fluidization velocity when $d_{av}=d_f$. Also, when $d_p >> d_f$ and considering that

$$(1-\varepsilon) x_f + \varepsilon = \varepsilon_p \tag{13}$$

by combination of Eq. (6), Eq. (7), Eq. (11) reduces to

$$-\frac{dP}{dz}=\rho_g g+\left(\rho_f-\rho_g\right)(1-\varepsilon)g\frac{x_f}{\varepsilon_p}=\rho_g g\frac{\varepsilon}{\varepsilon_p}+\rho_f(1-\varepsilon)g\frac{x_f}{\varepsilon_p}=\frac{\left(m_g+m_f\right)g}{AH_{fc}\varepsilon_p} \qquad (14)$$

Eq. (14) gives the pressure gradient in a conventional fluidized bed when the column cross-sectional area is $A\varepsilon_p$.

2.3 Pressure drop

Calculating the pressure drop across the confined bed is not straightforward. Intuitively, one would multiply the pressure gradient from Eq. (11) or Eq. (14) by the height of the packed-fluidized bed. However, this pressure drop must be equal to that across the packing alone when $x_f=0$, a condition not fulfilled by these relationships. Indeed, there is a crucial difference between a mixture of two solids that directly interact during the process of fluidization and a confined fluidized bed: in the former case any change of x_f leaves practically unchanged the height by which the pressure gradient is multiplied to obtain the total pressure drop; with the latter system, instead, the decrease of x_f is accompanied by the parallel reduction down to zero of the height of the finer component hosted in the voids of the coarser one, so that integration of the pressure gradient to obtain the total pressure drop becomes impossible.

Altogether this inconsistency stems from the non-interacting nature of the packed spheres, i.e. from the fact that fine particles can freely move within their interstitial voids. However, the absence of a direct interaction between the two components of the confined fluidized bed makes it possible to obtain a solution by considering only the force balances on the fluid and the fine solid. However, disregarding the force balance on the packed particles produces a lack of information on the geometry of the system. In this regard, Eq. (14) suggests that the collection of fine particles can be considered as a fluidized bed in a column of reduced cross-sectional area $A\varepsilon_p$ and with an internal voidage equal to ε. In these conditions, preserving the total fine mass requires the equivalent height of this bed to be:

$$H_f^{eq}=\frac{AH_{fc}(1-\varepsilon)x_f}{A\varepsilon_p(1-\varepsilon)}=\frac{H_{fc}x_f}{\varepsilon_p} \qquad (15)$$

and the contribution of the bed of fines to the dynamic pressure drop (i.e. devoid of the fluid hydrostatic head) can be calculated as:

$$-\Delta P_f = 180\frac{\mu_g u}{d_{av}^2}\frac{(1-\varepsilon)^2}{\varepsilon^3}\frac{H_{fc}x_f}{\varepsilon_p} \tag{16}$$

The contribution of the packing to the pressure drop can be obtained by eliminating the volumetric effect of the fine particles. In other words, the force balances on the fluid and the coarse solid, namely Eqs (2) and (4), can be rewritten with $\varepsilon=\varepsilon_p$, obtaining:

Gas
$$-\frac{dP}{dz}-\rho_g g-180\frac{\mu_g u}{d_{av}^2}\frac{(1-\varepsilon_p)^2}{\varepsilon_p^3}=0 \tag{17}$$

Packing
$$-\frac{dP}{dz}-\rho_p g+180\frac{\mu_g u}{d_{av}d_p}\frac{(1-\varepsilon_p)}{\varepsilon_p^2}+f_d=0 \tag{18}$$

In light of Eq. (16), the dynamic pressure drop due to dissipation on the packing particles can be expressed as:

$$-\Delta P_p = 180\frac{\mu_g u}{d_{av}^2}\frac{(1-\varepsilon_p)^2}{\varepsilon_p^3}H_{fc} \tag{19}$$

Thus, the total pressure drop is obtained by adding Eqs. (16) and (19) and the hydrostatic head of the fluid, yielding:

$$-\Delta P=(-\Delta P_g)+(-\Delta P_f)+(-\Delta P_p)=\rho_g g H_{fc}+180\frac{\mu_g u}{d_{av}^2}\frac{(1-\varepsilon)^2}{\varepsilon^3}\frac{H_{fc}x_f}{\varepsilon_p}+180\frac{\mu_g u}{d_{av}^2}\frac{(1-\varepsilon_p)^2}{\varepsilon_p^3}H_{fc} \tag{20}$$

At a first inspection, Eq. (20) appears to be inconsistent with the equation for the pressure drop in a binary-solid bed of non-interacting particles, derived elsewhere [6]. In reality, when two solid species are simultaneously fluidized, x_f becomes the volume fraction of the finer of the two non-interacting solids. In absence of packing, both x_f and ε_p are therefore equal to 1 and Eq. (20) reduces to:

$$-\Delta P=\rho_g g H_{fc}+180\frac{\mu_g u}{d_{av}^2}\frac{(1-\varepsilon)^2}{\varepsilon^3}H_{fc} \tag{21}$$

where d_{av} is in this case the average Sauter diameter of the two non-interacting solids.

In order to easily compare these results with what obtained with mixtures of non-interacting solids [2], the derivation of the previous expressions has resorted to the Carman-Kozeny's equation. However, the presence of the coarse packing spheres requires Ergun's equation to be used. In this case, Eq. (20) becomes:

$$-\Delta P = \rho_g g H_{fc} + \left[150 \frac{\mu_g u}{d_{av}^2} \frac{(1-\varepsilon)^2}{\varepsilon^3} + 1.75 \frac{\rho_g (1-\varepsilon) u^2}{\varepsilon^3 d_{av}} \right] \frac{H_{fc} x_f}{\varepsilon_p} + \left[150 \frac{\mu_g u}{d_{av}^2} \frac{(1-\varepsilon_p)^2}{\varepsilon_p^3} + 1.75 \frac{\rho_g (1-\varepsilon_p) u^2}{\varepsilon_p^3 d_{av}} \right] H_{fc} \quad (22)$$

As shown later on in this paper, Eq. (22) is used to predict the pressure drop in a packed-fluidized bed also beyond the onset of fluidization of the fine particles, given that the overall voidage of the packed-fluidized bed is lower than ε_p. The values of ε at $u>u_{mfc}$ were obtained by direct reading of the packed-fluidized bed height.

3. EXPERIMENTAL

The experiments were carried out in two different columns: the smaller of the two has an internal diameter of 5 cm and a packing made of lead spheres with a diameter of 4.1 mm; the larger one, 0.10 m ID, hosted a bed of glass spheres of 11 mm. In both cases the packing voidage was equal to 0.38. A high pressure drop porous plate was used as gas distributor. The fine particle bed was fluidized by air, whose flow rates were regulated by a set of rotameters covering the range 0-2600 Nl/h. The total pressure drop across the confined particle bed was measured by a U-tube water manometer.

Several cuts of glass ballotini, with size varying from 100 to about 600 μm were fluidized in the confined condition. Other spherical solids were also used, namely ceramic, zirconium oxide, steel and bronze; for all of them the cuts considered were 200-250 μm and 250-300 μm. Table 1 reports the properties of the experimental solids.

A weighed amount of fine spheres was poured onto the column within the voids of the packing to form a packed-fluidized bed with an aspect ratio H_{fc}/D never smaller than 2, a condition that ensures repeatability of the measurements of the minimum fluidization velocity [23]. Furthermore, the height of the bed is measured after a fluidization-defluidization cycle, in order to obtain a

repeatable initial state. Table 1 reports also the ratio between the particle diameter of the fine solids and the equivalent hydraulic diameter of the void network of the packed bed defined as

$$d_h = \frac{2}{3}\frac{\varepsilon_p}{(1-\varepsilon_p)} d_p \tag{23}$$

For the lead and glass spheres used to form the packing in the two different columns, d_h results equal to 0.168 and 0.453 cm respectively. The "relative voidage" ε_{fc} (i.e. the voidage that the fine bed would have in a column of section $A\varepsilon_p$), which can be compared with the bed voidage ε_f in a conventional fluidization column, has been determined as the ratio between the absolute voidage ε (defined by Eq. (9)) and that of the packing, ε_p. This comparison is illustrated in Fig. 2, at varying size ratio d_f/d_h (for the sake of clarity only the data relevant to glass ballotini are reported). It is noticed that for a given size of the packed spheres the increase of d_f leads to a more permeable particle matrix, as a result of the growing difficulty of filling the packed bed voids with the finer particles. At the same time, it is found that solids of different density give place to the same relative voidage (see Table 1). An exception is provided by ceramic spheres, apparently affected by electrostatic phenomena during expansion.

Before to apply the model previously illustrated to the experimental solids, values of the relative voidage for all solids have been calculated as a function of d_f/d_h by the following correlation (obtained by experimental data regression and shown in Fig. 2)

$$\varepsilon_{fc} = -0.24\left(\frac{d_f}{d_h}\right)^2 + 0.56\left(\frac{d_f}{d_h}\right) + 0.38 \tag{24}$$

and the relevant values have also been included in Table 1.

4. RESULTS AND DISCUSSION

Prior to experiments on confined fluidized beds, the pressure drop across the fixed packing alone has been measured. For both types of coarse materials used, i.e. lead spheres and glass ballotini, Ergun equation gives accurate predictions of ΔP, as shown by Fig. 3. Such a verification makes it possible to calculate ΔP_{ep} after measuring the height of the confined bed. This value is then

subtracted to the experimental value of ΔP_{tot}, in a way that the pressure drop across the confined fluidized bed ΔP_{conf} (see again Fig. 1) is evaluated as

$$\Delta P_{conf} = \Delta P_{tot} - \Delta P_{ep} \tag{25}$$

Thus, the diagrams of Fig. 4 report the trend of the pressure drop across the confined bed (ΔP_{conf}) and that of the voidage ε versus the superficial gas velocity.

Data of Fig. 4(a) were obtained in the 5 cm column packed with lead spheres, with GB136 μm and BR229 μm as confined fluidized particles. Although log-log diagrams do not illustrate that clearly, a different behaviour is observed in the particulate fluidization of the two solids: bronze particles exhibit more regular homogeneous expansion, which starts at a definite value of u_{mfc}; the voidage variation follows a unique power law and the corresponding pressure drop is described by Ergun's equation, in the form of Eq. (22). On the other hand, glass ballotini do not show an equally sharp transition to homogeneous fluidization. Moreover, their expansion follows two distinct trends: at relatively low velocity the pressure drop tends to remain constant like in conventional fluidization, whereas a monotonic increase is observed at higher velocities.

Data of Fig. 4(b) are relevant to fluidization of GB 100 μm in the 5 cm column and to that of GB 319 μm in the 10 cm column; their behaviour is fully similar to that of GB 136 μm described above. For these two systems, d_h results equal to 1.68 and 4.53 mm, respectively, but the corresponding d_f/d_h ratios are very close. In more general terms, it can be stated that solids for which the ratio d_f/d_h is lower than about 0.1 display an anomalous regime of homogeneous expansion. This is the case of the three finest cuts of GB in the 5 cm column and of the two finest cuts in the 10 cm column. A possible interpretation of this finding is that in their fixed state small particles can penetrate the voids of the packing more deeply than bigger ones, up to the region around the contact points between the coarse spheres. It may be thought, therefore, that at relatively low velocities the amount of particles involved in the expansion process is somewhat limited and that higher velocities are required to mobilize the whole mass of fines.

Finally, inspection of Fig. 4(c), which reports results relevant to solids of noticeably different density (2480 kg/m^3 for glass ballotini and 6150 kg/m^3 for spheres of zirconium oxide), shows that for

solids of comparable size neither the trend of the pressure drop variation nor that of the bed expansion is affected by the density variation.

To illustrate the dependence of the minimum fluidization velocity of the confined bed on particle diameter, Fig. 5 compares data of u_{mfc} of glass ballotini with those of conventional u_{mf}. It may be observed that the transition to the fluidized state of the confined bed occurs at lower velocities, so that u_{mfc} is at least half the value of u_{mf}. At the same time, the dependence of the minimum fluidization velocity of the confined bed on particle density keeps on being linear, as demonstrated by Fig. 6.

The minimum fluidization velocities of the fine solids in the confined condition predicted by Eq.(12) are reported in the last column of Table 1 and then compared with the experimental values of u_{mfc} in Fig. 7. The error is generally lower than 15% while the maximum divergence is about 20%. Altogether, in spite of some deviations, the model is in good agreement with the experiments over a wide range of conditions.

Equation (22) has also been used to predict the variation of the pressure drop with gas velocity. To this regard, Fig. 8 compares the experimental values of ΔP_{conf} with its predictions. The three systems referred to in these plots are an example of how a satisfactory agreement between experimental data and model predictions is normally obtained. It may also be noticed that this agreement is not impeded by the simplification inherent in using the Ergun's equation at high solid fractions, as it is generally accepted that a slightly different dependence on voidage should be considered at values significantly far from 0.6 [26]. Nevertheless, the comparison between model predictions and experimental data demonstrates that the theory based on separate force balances succeeds in describing the fluidization process in a confined environment.

In this way this study extends to confined fluidized beds the approach originally proposed for two-solid mixtures whose components undergo fluidization simultaneously [6]. With both categories of systems the role played by solid-solid interaction in determining the mechanism of fluidization is crucial, although the nature of this interaction is not the same. In a confined environment the presence of the packing modifies the fluid flow and, indirectly, the drag force exerted on the fine solids. On the other hand, when mixtures of solids with comparable values of u_{mf} are fluidized, an

additional force is directly exchanged between the two phases. The approach followed in this study proves therefore capable of identifying the forces at work during the process and sheds some light on its essential features.

CONCLUSIONS

The validity of the novel theoretical approach followed in this paper, based on writing separate force balances on the different phases of a confined fluidized bed, has been established by comparison of its predictions with a large number of experimental data. Over a wide range of conditions, including the variation of density and size of the fluidized particles as well as that of the diameter of the packed spheres and of the fluidization column, the model proposed calculates with good accuracy the pressure drop across the bed at varying velocity both in the fixed and in the suspended state. From it, the minimum fluidization velocity of the fine particles in the voids of the coarser packing is predicted with a satisfactoy degree of precision

The results obtained extend the range of application of a model originating from the analysis of multicomponent fluidization and provide a firm basis to representation of the phenomenology of confined fluidization.

NOMENCLATURE

A	column cross-sectional area, cm^2
b_i	the body forces per unit volume on the i^{th} component, N/m^3
D	column internal diameter, cm
d_{av}	Sauter mean diameter, μm
d_f	fine solid diameter, μm
d_h	hydraulic diameter of the voids , mm
d_p	diameter of the packed solid, mm
f_d	drag force per unit volume of fluid, N/m^3
f_i	the average surface forces per unit volume on the i^{th} component, N/m^3
g	gravity acceleration, m/s^2
H_{fc}	confined bed height, cm
H_f^{eq}	equivalent bed height, cm
H_p	packed bed height, cm
$m_{f/p}$	mass of the fine /packed solid, kg
P	pressure, Pa
u	superficial gas velocity, cm/s
u_{mf}	minimum fluidization velocity of the conventional bed, cm/s
u_{mfc}	minimum fluidization velocity of the confined bed, cm/s
z	vertical distance above the distributor, cm
$x_{f/p}$	volume fraction of the fine/packed component in the solid mass, -

Greek symbols

$\alpha_{f/p}$	volume fraction of the fine /packed solid, -
ΔP_{conf}	pressure drop in the confined system, Pa
ΔP_{ep}	pressure drop in the empty packing, Pa
ΔP_{tot}	pressure drop in the whole system, Pa
ε	voidage of the packed-fluidized bed, -

ε_f	voidage of the fine solid in a conventional bed, -
ε_{fc}	voidage of the equivalent conventional bed $\varepsilon/\varepsilon_p$, -
ε_p	voidage of the packed bed, -
μ_g	gas viscosity, (kg/m s)
$\rho_{f/p}$	density of the fine /packed solid, kg/m^3
ρ_g	gas density, kg/m^3

Subscripts

g	of the gas
f	of the fine solid
p	of the packed solid

REFERENCES

[1] P.N. Rowe, A.W. Nienow, Minimum fluidization velocity of multicomponent particle mixtures, Chem. Eng. Sci. 29 (1975) 1365-1369.

[2] B. Formisani, R. Girimonte, Experimental analysis of the fluidization process of binary mixtures of solids, KONA Powder and Particle Journal 21 (2003) 66-75.

[3] D.C. Sau, S. Mohanty, K.C. Biswal, Prediction of critical fluidization velocity and maximum bed pressure drop for binary mixture of regular particles in gas-solid tapered fluidized beds, Chemical Engineering and Processing 47 (2008) 2114-2120.

[4] Mohammad Asif, Effect of volume-contraction on incipient fluidization of binary-solid mixtures, Powder Technology 9 (2011) 101-106.

[5] Basu Paudel, Zhi-Gang Feng, Prediction of minimum fluidization velocity for binary mixtures of biomass and inert particles, Powder Technology 237 (2013) 134-140.

[6] B. Formisani, R. Girimonte, V. Vivacqua, The interaction between mixture components in the mechanism of binary fluidization, Powder Technology 266 (2014) 228–235.

[7] F.P. Di Maio, R. Di Renzo, V. Vivacqua, A particle segregation model for gas fluidization of binary mixtures, Powder Technololology 226 (2012) 180–188.

[8] B. Formisani, R. Girimonte, V. Vivacqua, Fluidization of mixtures of two solids differing in density or size, AIChE J. 57 (2011) 2325–2333.

[9] B. Formisani, R. Girimonte, V. Vivacqua, Fluidization of mixtures of two solids: a unified model of the transition to the fluidized state, AIChE J. 59 (2013) 729–735.

[10] R. Girimonte, V. Vivacqua, The expansion process of particle beds fluidized in the voids of a packing of coarse spheres, Powder Technology 213 (2011) 63–69.

[11] Mandal D., Sathiyamoorthy D., Vinjamur M., Heat Transfer Characteristics of Lithium-Titanate Particles in Gas-Solid Packed Fluidized Bed, Fusion Sci. Technol, 62(1) (2012), 150-156.

[12] D. Mandal, D. Sathiyamoorthy, M. Vinjamur, Experimental Measurement of Effective Thermal Conductivity of Packed Lithium-Titanate Pebble Bed, Fusion Eng. Des. 87 (2012), 67-76.

[13] D. Mandal, D. Sathiyamoorthy, M. Vinjamur, Hydrodynamics of Beds of Small Particles in the Voids of Coarse Particles, Powder Technol., 235 (2013), 256-262.

[14] X. Song, Z. Wang, Y. Jin, Z. Tanaka, Gas-solid circulating fluidization in a packed bed, Powder Technology 83 (1995) 127–131.

[15] A.G.J. van der Ham, W. Prins, W.P.M. van Swaaij, A small-scale regularly packed circulating fluidized bed Part I: Hydrodynamics, Powder Technology 79 (1994) 17–28.

[16] A.G.J. van der Ham, W. Prins, W.P.M. van Swaaij, A small-scale regularly packed circulating fluidized bed Part II: Mass transfer, Powder Technology 79 (1994) 29–41.

[17] Y. Ding, Z. Wang, D. Wen, M. Ghadiri, X. Fan, D. Parker, Solids behaviour in a gas solid two-phase mixture flowing through a packed particle bed, Chem. Eng. Sci. 60 (2005) 5231–5239.

[18] A. Delebarre, B. Bitaud, M.C. Regnier, Gas-solid suspension flowing through a granular bed, Powder Technology 91 (1997) 229–236.

[19] P. Glasserman, D. Videla, U. Bohm, Liquid fluidization of particle in packed beds, Powder Technology 79 (1994) 237–245.

[20] G. Donsì, G. Ferrari, B. Formisani, Expansion behavior of confined fluidized beds of fine particles, Can. J. Chem. Eng. 67 (1989) 185–190.

[21] D. Mandal, V. K. Sharma, H. J. Pant, D. Sathiyamoorthy, M. Vinjamur, Quality of Fluidization in Gas-Solid Fluidized and Packed Fluidized Bed - an Experimental Study using Gamma-Ray Transmission Technique, Powder Technology 226 (2012) 91-98.

[22] D. Mandal, D. Sathiyamoorthy, M. Vinjamur, Experimental investigation of heat transfer in gas–solid packed fluidized bed, Powder Technology 246 (2013) 252–268.

[23] R. Girimonte, V. Vivacqua, Design criteria for homogeneous fluidization of Geldart's class B solids upward through a packed bed, Powder Technology 249 (2013) 316–322.

[24] G.B. Wallis, One-dimensional Two-phase Flow, McGraw-Hill, Inc., New York, 1969.

[25] S. Ergun. Fluid Flow through Packed Columns. Chem. Eng. Prog., 48(2):89-94, 1952.

[26] L.G. Gibilaro, Fluidization-dynamics, Butterworth-Heinemann, Oxford, 2001.

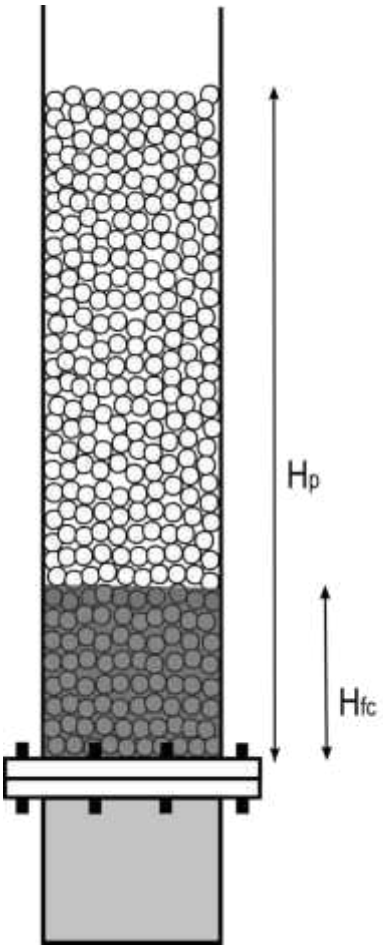

Fig.1 - Schematic structure of a packed fluidized bed.

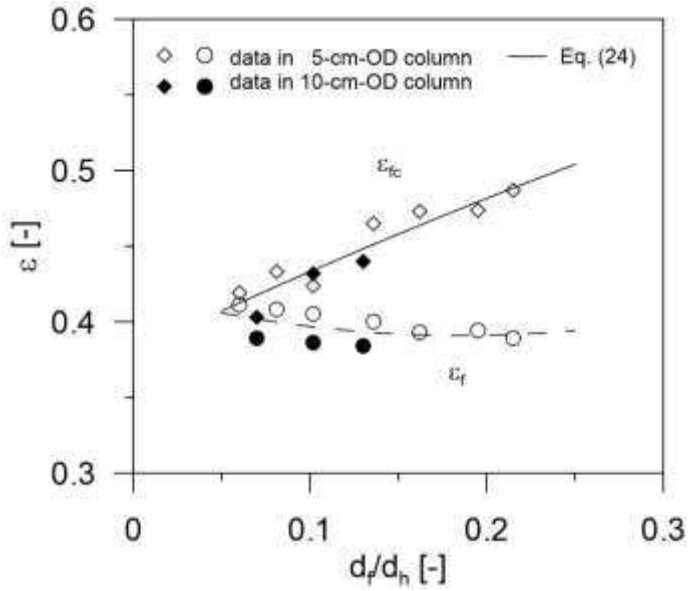

Fig.2 - Comparison between the trend of the relative voidage ε_{fc} versus d_f/d_h and that the conventional bed voidage ε_f (full symbols are GB solids investigated in the 10 cm OD column).

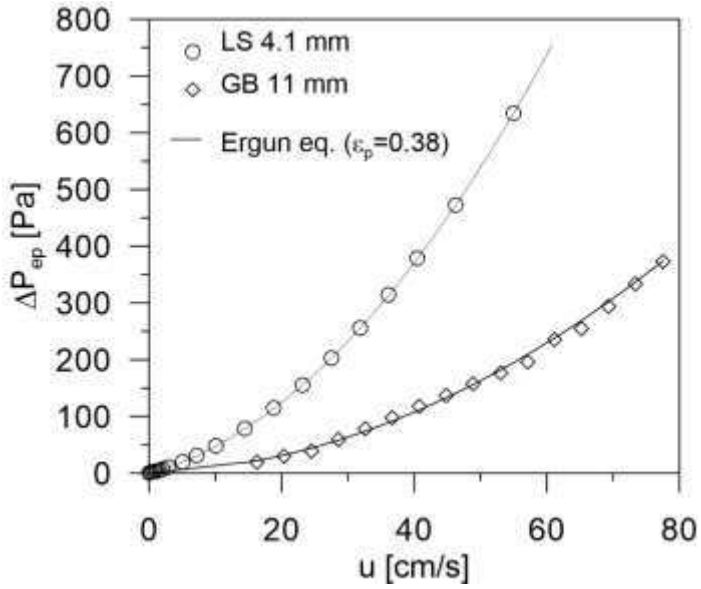

Fig.3 - Prediction of the pressure drop across the empty packings by Ergun equation.

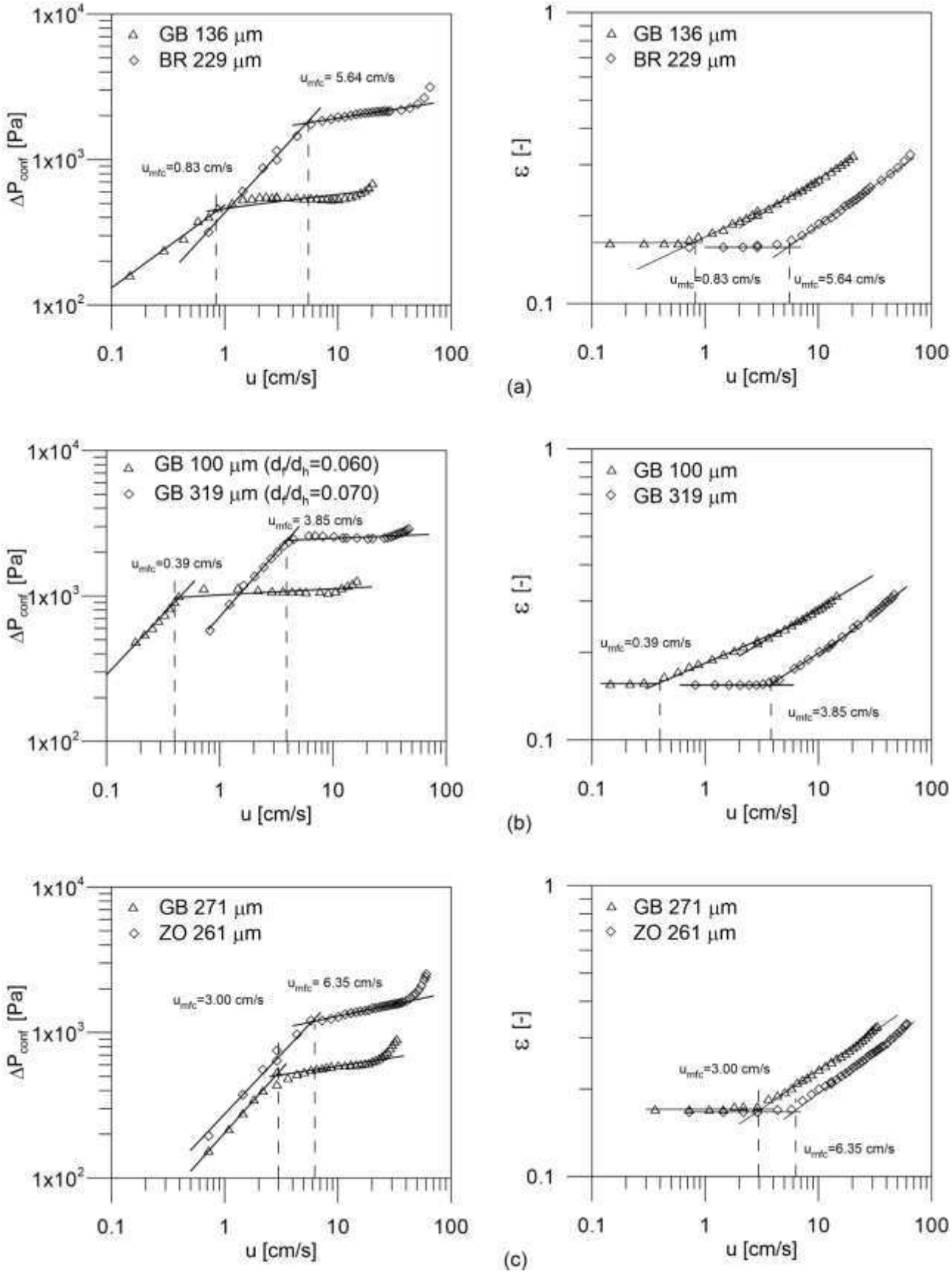

Fig.4 - Typical experimental variation of the pressure drop and voidage with fluidization velocity.

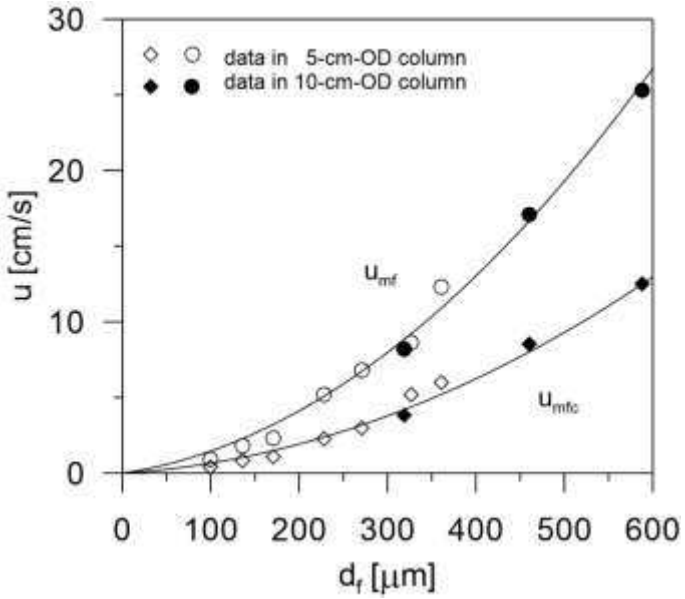

Fig.5 - Comparison between the minimum fluidization velocity in the conventional and confined bed (full symbols are GB solids investigated in the 10 cm OD column).

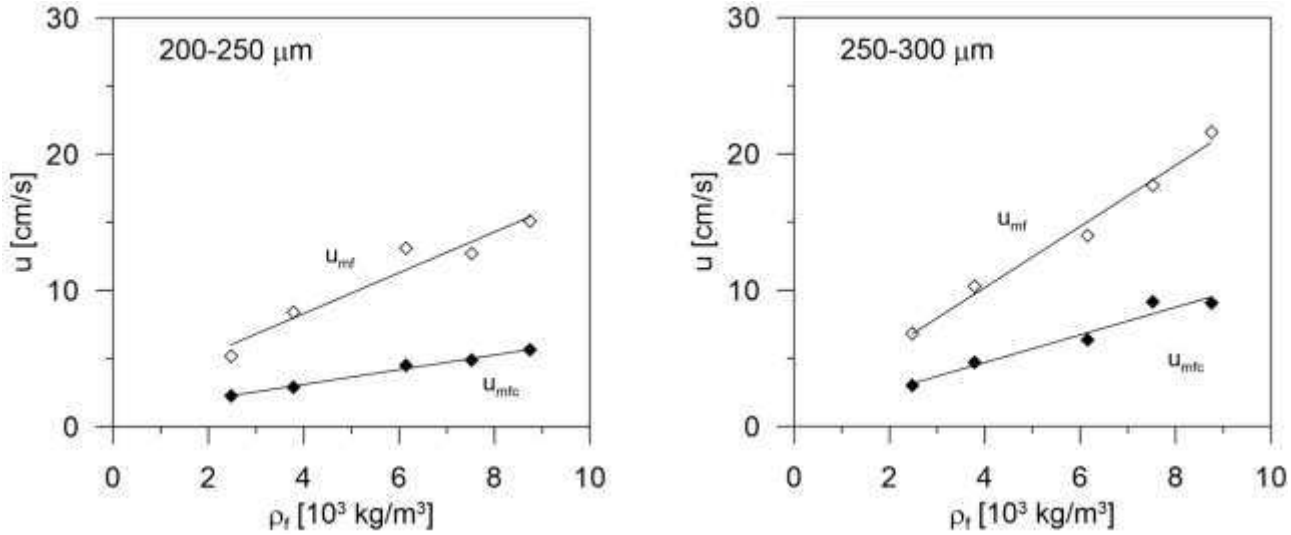

Fig.6 - Effect of particle density on the confined minimum fluidization velocity.

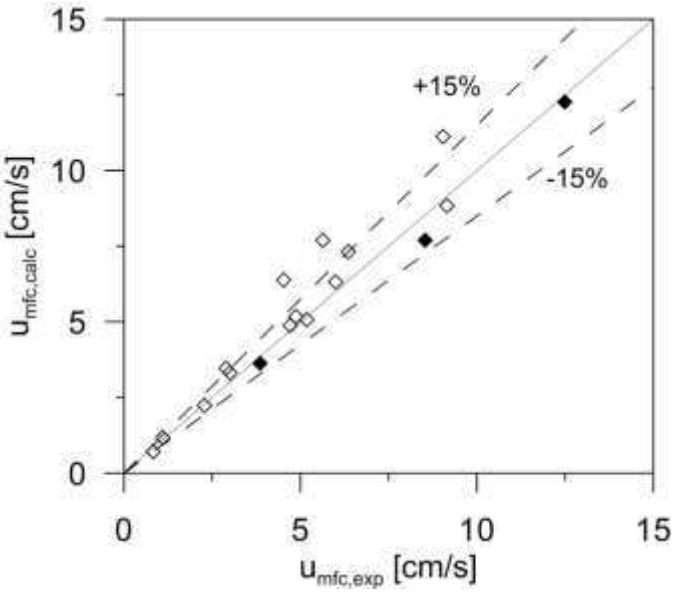

Fig.7 - Comparison between experimental and calculated values of the minimum fluidization velocity in confined bed.

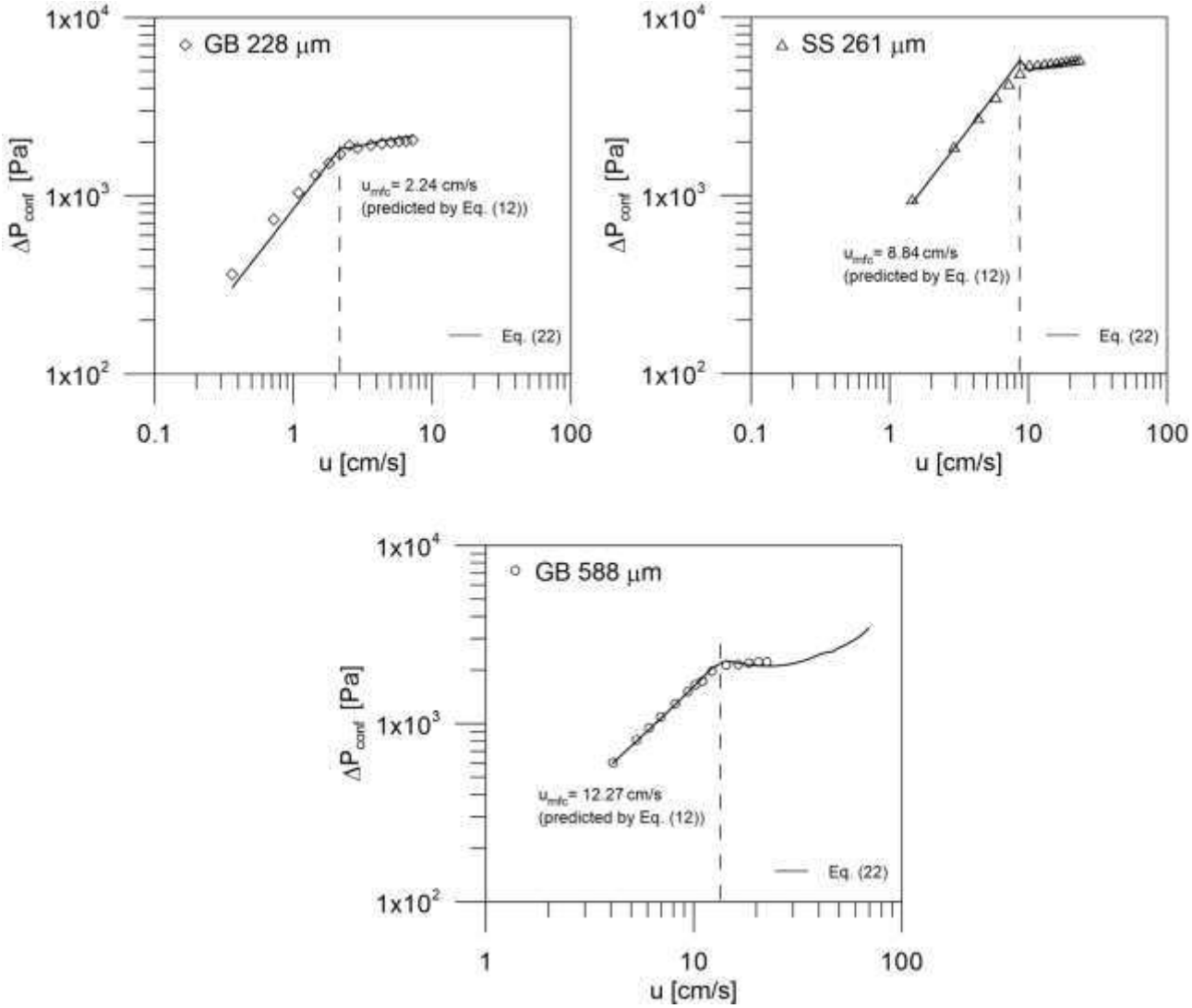

Fig.8 - Prediction of the pressure drop in confined bed in function of velocity by Eq. (22).

Table 1 - Fluidization properties of the experimental solids.

	Particle density ρ_f [kg/m^3]	Sauter diameter d_f [μm]	d_f/d_h [-]	Conventional		Confined		Predicted	
				u_{mf} [cm/s]	ε_f [-]	ε_{fc} [-]	u_{mfc} [cm/s]	ε_{fc} (Eq.(24)) [-]	u_{mfc} (Eq. (12)) [cm/s]
GB 90-125 μm	2480	100	0.060	0.9	0.411	0.419	0.39	0.412	0.36
GB 125-150 μm		136	0.082	1.8	0.408	0.433	0.83	0.424	0.70
GB 150-200 μm		171	0.103	2.3	0.405	0.424	1.10	0.434	1.17
GB 200-250 μm		228	0.137	5.2	0.400	0.465	2.27	0.451	2.24
GB 250-300 μm		271	0.163	6.8	0.393	0.473	3.00	0.464	3.32
GB 300-355 μm		327	0.197	8.6	0.394	0.474	5.18	0.479	5.08
GB 355-400 μm		361	0.218	12.3	0.389	0.487	6.00	0.489	6.32
GB 300-355μm		319	0.070	8.2	0.389	0.403	3.85	0.418	3.64
GB 400-500μm		460	0.102	17.1	0.386	0.432	8.54	0.434	7.70
GB 560-630μm		588	0.130	25.3	0.384	0.440	12.5	0.448	12.27
CE 200-250 μm	3780	230	0.139	8.4	0.399	0.412	2.89	0.452	3.46
CE 250-300 μm		268	0.161	10.3	0.396	0.448	4.70	0.463	4.87
ZO 200-250 μm	6150	245	0.148	12.4	0.391	0.465	4.52	0.456	6.38
ZO 250-300 μm		261	0.157	14.0	0.386	0.473	6.35	0.461	7.32
SS 200-250 μm	7520	204	0.121	12.7	0.400	0.465	4.88	0.444	5.17
SS 250-300 μm		261	0.155	17.7	0.393	0.473	9.15	0.461	8.84
BR 200-250 μm	8750	229	0.138	16.3	0.399	0.465	5.64	0.451	7.70
BR 250-300 μm		272	0.164	21.6	0.394	0.473	9.04	0.464	11.12

GB glass ballotini, CE ceramic, ZO zirconium oxide, BR bronze, SS steel and LS lead spheres

Solids in bold are investigated in the 10-cm-OD column with a 11-mm-GB packing.